

# Periodicity staircase in a Fe/Gd magnetic thin film

Arnab Singh,<sup>1,\*</sup> Junli Li,<sup>2,\*</sup> Sergio A. Montoya,<sup>3</sup> Sophie Morley,<sup>4</sup> Peter Fischer,<sup>1,5</sup> Steve D. Kevan,<sup>4</sup> Eric E. Fullerton,<sup>3</sup> Dao-Xin Yao,<sup>2,6,†</sup> Trinanjan Datta,<sup>7,8,‡</sup> and Sujoy Roy<sup>4,§</sup>

<sup>1</sup>*Materials Science Division, Lawrence Berkeley National Laboratory, Berkeley, California 94720, USA*

<sup>2</sup>*State Key Laboratory of Optoelectronic Materials and Technologies,*

*Guangdong Provincial Key Laboratory of Magnetoelectric Physics and Devices,*

*Center for Neutron Science and Technology, School of Physics, Sun Yat-Sen University, Guangzhou 510275, China*

<sup>3</sup>*Center for Magnetic Recording Research, University of California San Diego, La Jolla Ca, USA*

<sup>4</sup>*Advanced Light Source, Lawrence Berkeley National Laboratory, Berkeley, California 94720, USA*

<sup>5</sup>*Department of Physics, University of California Santa Cruz, Santa Cruz CA, USA*

<sup>6</sup>*International Quantum Academy, Shenzhen 518048, China*

<sup>7</sup>*Department of Physics and Biophysics, Augusta University, 1120 15th Street, Augusta, Georgia 30912, USA*

<sup>8</sup>*Kavli Institute for Theoretical Physics, University of California, Santa Barbara, California 93106, USA*

Presence of multiple competing periodicities may result in a system to go through states with modulated periodicities, an example of which is the self-similar staircase-like structure called the Devil's staircase. Herein we report on a novel staircase structure of domain periodicity in an amorphous and achiral Fe/Gd magnetic thin film wherein the reciprocal space wavevector  $\mathbf{Q}$  due to the ordered stripe domains does not evolve continuously, rather exhibits a staircase structure. Resonant X-ray scattering experiments show jumps in the periodicity of the stripe domains as a function of an external magnetic field. When resolved in components, the step change along  $Q_x$  was found to be an integral multiple of a minimum step height of 7 nm, which resembles closely to the exchange length of the system. Modeling the magnetic texture in the Fe/Gd thin film as an achiral spin arrangement, we have been able to reproduce the steps in the magnetization using a Landau-Lifshitz spin dynamics calculation. Our results indicate that anisotropy and not the dipolar interaction is the dominant cause for the staircase pattern, thereby revealing the effect of achiral magnetism.

## Introduction.

Appearance of staircase-like structure is a fascinating phenomenon that is observed in a variety of condensed matter systems. In 2D electron gas, quantized conductance is manifested as step feature in Hall effect measurements [1]. In quantum materials, interplay of competing interactions with multiple periodicities in a system can give rise to a ground state whose length scales are defined by the modulation of the original periodicities. Example of such modulated periodicities include commensurate and incommensurate phases, such as density waves in solids [2], stripes and charge density waves in cuprate superconductors [3–5], charge ordered state in manganites [6], and helical spin structure in magnetic systems [7]. A well known staircase structure is the Devil's staircase which appears when a system goes through numerous phase-locked modulated periodicities [8–10]. Devil's staircase have been observed in magnetic systems [8, 11–14], liquid crystals [15] and in ferroelectrics [16]. Apart from fundamental science the staircase structures have potential applications such as in metrology, sensing devices etc [17].

Interesting staircase structure in domain size and in magnetoresistance have been observed in Dzyaloshinskii-Moriya interaction (DMI) based solitonic system [18, 19] Competition between symmetric exchange interaction and the anti-symmetric Dzyaloshinskii-Moriya interaction (DMI) can give rise to interesting magnetic phases such as helix, stripes and

skyrmion phases appear [11, 20–22]. DMI based chiral magnetic order in helimagnet is called Dzyaloshinskii type helimagnet structure, while a helical magnetic order due to competition between ferromagnetic and antiferromagnetic exchange interaction is known as helimagnetic structure of the Yoshimori type [23]. The chiral magnetic structures in a helimagnet exhibits solitons that can be manipulated by an external magnetic field [24]. More specifically, the soliton periodicity changes in a step wise manner which is attributed to the discrete changes in the soliton number because of confinement at the grain boundaries [24, 25]. Field evolution of confined helicoids have also been shown to occur via discrete steps in helical magnet MnSi [26]. The thin film structure of MnSi accommodates a finite number of turns and the jumps are explained due to annihilation of individual turns of the helicoid.

In this article we report on the appearance of staircase structure of the scattering wave vector  $\mathbf{Q}$  due to the ordered stripe domains in an amorphous Fe/Gd thin film. In contrast to the single crystals with DMI as described in the previous paragraph, the amorphous Fe/Gd thin film is a perpendicular magnetic anisotropy (PMA) system with dominant dipolar interactions and negligible DMI [27]. The presence of dipolar interactions can support an achiral phase which in the stripe phase results in the spins to reverse its direction of orientation twice within a period, resulting in no net chirality. We performed resonant coherent soft X-ray scattering to study variations of aligned stripe-domains periodicity. Depending on the applied field condition it is possible to obtain a skyrmion lattice phase that consists of equal number of skyrmions with opposite chiralities (+1 and -1) [28]. We observed that the scattering wave vector  $\mathbf{Q}$  changes in steps with no well defined step height and

\* These two authors contributed equally.

† Corresponding author: yaodaax@mail.sysu.edu.cn

‡ Corresponding author: tdatta@augusta.edu

§ Corresponding author: sroy@lbl.gov

width. However, when  $\mathbf{Q}$  is resolved into components  $Q_x$  and  $Q_y$ , the steps along  $Q_x$ , were found to be in integer multiple of 7 nm, which is close to the exchange length of the system. At higher temperature the steps were smeared due to thermal fluctuations.

Our X-ray scattering studies have been complemented by spin dynamics calculations that take into account the achiral nature of the system. We have simulated an experimentally observed (non-equilibrium) process where a global versus local domain dynamics delicately balances each other. On one hand we have the divergence in the total periodicity of the stripes with increasing magnetic field. On the other hand this is being counter balanced by the local minority stripe width which cannot fall below a certain size. Thus, instead of a bulk macroscopic motion of domain walls over the entire sample, these competing tendencies cause the local forces and energetics experienced by the minority domains to locally annihilate some of these half-periods. This in turn leads to (as observed experimentally and verified theoretically) a local readjustment of the domain sizes. By defining two length scales related to global and local achirality, we have been able to theoretically generate steps as a function of applied magnetic field and show the important role that anisotropy plays in generating the steps in these systems. We have developed a theoretical model for the appearance of steps using exchange, dipole and anisotropy. Our calculations indicate that the origin of the steps lie in the anisotropy term. Even if exchange and dipole interactions are present, absence of anisotropy does not produce steps. Thus, although the appearance of steps do look similar in single crystal DMI material and amorphous Fe/Gd sample, the physical origin of the steps in the two systems are different.

## Results.

### Resonant Scattering due to Stripes

The scattering geometry for the experimental set-up is shown in Fig.1(a). X-ray beam whose energy is tuned to the Fe  $L_3$  edge is incident normally on the sample. A pinhole was placed on the beam path upstream 5 mm from the sample to establish transverse coherence of the beam. In this geometry the X-ray photons are sensitive to the spins that are aligned along the beam direction. The scattering pattern was collected on a charge coupled device camera (CCD) placed about 0.5 m away downstream. Resonant X-ray scattering measurements are sensitive to static magnetic structure ( $S(\mathbf{q})$ ) and spatial correlation length ( $\xi_s$ ). From the position and intensity of the Bragg peaks it is possible to extract information about the periodicity and strength of the magnetic order. Fig.1(b) shows the full field X-ray microscope images (top panel) and X-ray resonant scattering pattern (bottom panel) of the sample. We observed three distinct magnetic phases, namely, disordered stripe, ordered stripe and skyrmions, which can be obtained by either varying the temperature or applied magnetic field. The X-ray real space images were obtained by varying the applied magnetic field at 300 K, while the resonant X-ray scattering data was measured from  $LN_2$  temperatures to room temperature as a function of the applied magnetic field. In the ordered stripe phase ( $T = 239\text{K}$ ) the domain periodicity ( $2\pi/Q$ ) at remanence is  $(119 \pm 5)$  nm. The stripe pattern persists as the

field is increased from zero till around 170 mT, when new peaks in a distorted hexagonal pattern start to appear indicating a transition to the skyrmion phase. These observations are consistent with previous reports [27–29].

Fig.1(c) shows the behavior of the integrated intensity of 1<sup>st</sup> and 2<sup>nd</sup> order diffraction peak from the ordered stripe domains. As the applied magnetic field is increased the 1<sup>st</sup> order peak is maximum and the 2<sup>nd</sup> order is minimum. This is because of the equal width of up and down domains. Applied out-of-plane magnetic fields break this symmetry, causing even order diffraction peaks to appear. Around 170 mT,

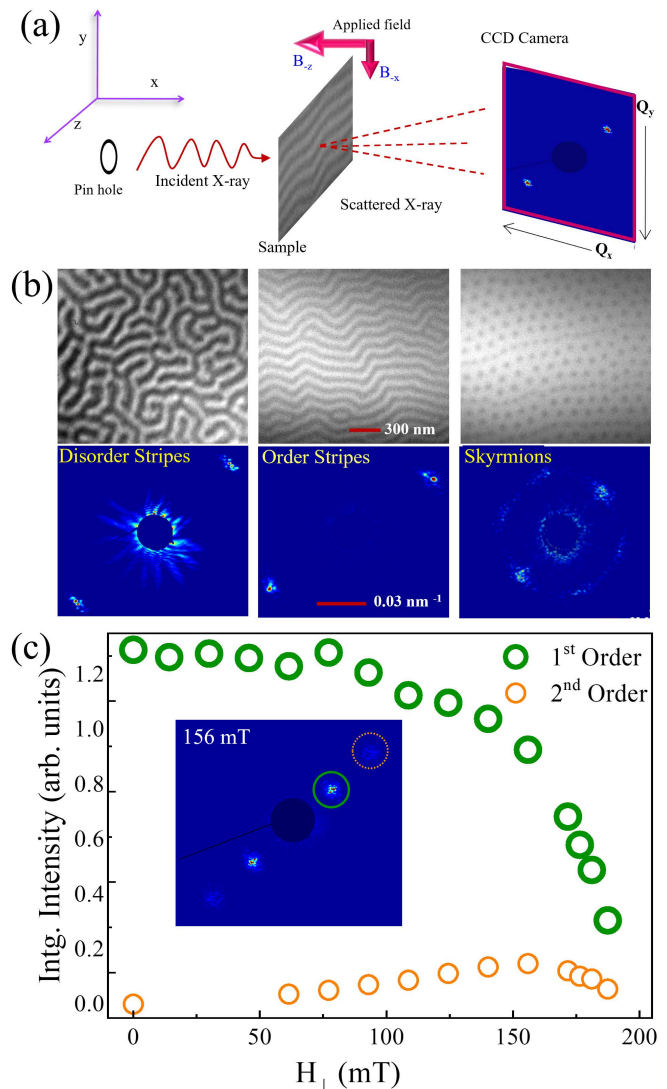


FIG. 1. **Experimental set-up and magnetic phases.** (a) Schematic of the coherent magnetic X-ray scattering geometry. (b) Real space (top panel) and reciprocal space (lower panel) of the different magnetic phases present in a Fe/Gd thin film. The scattering images were taken at  $H = 0\text{mT}$ ;  $T = 85\text{K}$  (disorder stripes),  $H = 0\text{mT}$ ;  $T = 225\text{K}$  (order stripes) and  $H = 190\text{mT}$ ;  $T = 239\text{K}$  (skyrmions). (c) Variation of the 1st and 2nd order magnetic diffraction peak with field at 239K. Inset image shows the appearance of both 1st and 2nd order diffraction peaks

intensity of both peaks start to diminish and eventually new peaks in the form of hexagonal pattern appear (see Fig.1(b), bottom panel). It is interesting to note that in the hexagonal phase we observe two relatively strong intensity spots along the same direction as the stripes which would indicate that somehow the original direction of the stripes is retained even in the hexagonal phase.

### Staircase Structure of Q-vector

The evolution of the stripe-diffraction spot in Q-space is shown in Fig.2(a) as a function of the applied field at  $T = 230$  K. At the start of the field cycle, the momentum transfer vector is  $Q_1 (= 0.052 \text{ nm}^{-1})$ . As the field increases, the magnetization increases and the size of the favorable domains (along the field directions) also increases leading to an increased domain periodicity resulting in a smaller Q-value. Interestingly, we observed that the Q-value corresponding to the magnetic Bragg peak decreases in discrete steps as a function of applied magnetic field giving rise to a staircase-like structure.

The evolution of domain periodicity happens in several steps that involve sudden jumps and appearance of a modulated periodicities. We find that along with the main magnetic Bragg peak, a much weaker satellite peak develop at a smaller Q-value, and both the peaks evolve in an interesting way as the field is changed. The increase in field leads to first the appearance of an initially weaker intensity satellite peak at  $Q_2$  (at a smaller value than zero field Bragg peak at  $Q_1$ ). With further increase in the field, the main Bragg peak ( $Q_1$ ) suddenly merges with  $Q_2$  giving rise to a step-like feature. Since the position and intensity of the Bragg peak gives the periodicity of the stripe domains and strength of domain scattering, we can conclude that the number of domains with periodicity  $P_1 = 2\pi/Q_1$  decreases with increase in field while the number of domains of periodicity  $P_2 = 2\pi/Q_2$  starts to increase and finally all the domains suddenly transform to the periodicity  $P_2$ . This sequence of events, changing Q from  $Q_1$  to  $Q_7$  with a similar mechanism of peak shifts ( $Q_1 \rightarrow Q_2$ ;  $Q_3 \rightarrow Q_4$ ;  $Q_5 \rightarrow Q_6$ ) was observed throughout the stripe phase (see Fig. 2(a)). In some cases, a direct change in Q-values corresponding to the Bragg peaks without any satellite ( $Q_2 \rightarrow Q_3$ ;  $Q_4 \rightarrow Q_5$ ) was also observed.

In Fig.2(b) we convert the wavevector into real space periodicity ( $2\pi/Q$ ) and plot it as a function of applied field at different temperatures. At higher temperatures the total number of steps increase which results in the appearance of the first step at much lower fields for higher temperatures than the lower ones. The plot of the correlation values of the stripe-diffraction spot at different fields with respect to the one at remanence for increasing magnetic fields is shown in Fig.2(c). Any subtle changes in the speckle pattern between two frames taken at 0 mT and H mT will result in a value of the correlation coefficient (CC) which is defined by

$$CC = \frac{\sum_m \sum_n (A_{mn} - \bar{A})(B_{mn} - \bar{B})}{\sqrt{(\sum_m \sum_n (A_{mn} - \bar{A})^2)} \sqrt{(\sum_m \sum_n (B_{mn} - \bar{B})^2)}}, \quad (1)$$

where  $A$  and  $B$  corresponds to the two images taken at two different field values.  $A_{mn}$  denotes the intensity value of the pixel position at  $m^{\text{th}}$  row and  $n^{\text{th}}$  column of the 2D scattering

image.  $\bar{A}$  is the mean value of the 2D image. If  $CC=1$  then the two images are perfectly correlated,  $CC=0$  means completely de-correlated and  $CC$  values lying between 0 and 1 means partially correlated. Thus the variation of the correlation-coefficient can be attributed in the real space as either change in magnetization or density or periodicity of the stripes or any combination of these factors with applied field. In Fig.2(c) the  $CC$  is calculated between the scattering image taken at remanence (zero field) and another image taken at higher field. In this way the  $CC$  plot in Fig.2(c) is generated with increasing field with respect to zero field. The correlation coefficient also exhibits steps like behaviour (blue color line). As a measure of control parameter we also calculated correlation coefficients for the Airy pattern, which remains fairly close to unity at all the fields.

### Resolving staircase along $Q_x$ and $Q_y$ direction

A typical diffraction pattern containing only the centrosymmetric first order peaks is represented in Fig.3(a) along with their in-plane Q-vectors. The enlarged image of the diffraction spot in Fig.3(b) exhibit modulation with speckles indicative of heterogeneity in the magnetic phase. The diffraction spots appears at about  $45^\circ$  to the beam propagation direction (see Fig.3(a)), meaning domains are oriented  $45^\circ$  to the X-ray propagation direction. This is due to the presence of a small in-plane field. We resolved the resultant Q-vector along  $Q_x$  and  $Q_y$  components, to get information about change in the stripe periodicity along real space X and Y direction thereby obtaining real space value  $L_x$  and  $L_y$  as shown in the schematic representation in Fig.2(c). We find that the steps along  $L_x$  are significantly distinct compared to that in the  $L_y$  direction (see Fig.3(d and e)).

Interestingly, we found that the steps along  $L_x$  change in multiples of 7 nm. That is, the minimum change in periodicity along  $L_x$  is 7 nm. No such relationship was found in the  $L_y$  direction. The magnitude of the change in  $L_y$  is small and random compared to  $L_x$  (Fig.2 (d,e)). A schematic of a possible stripe domain arrangement is shown in Fig. 3(c). The blue (red) domains are majority (minority) domains. The stripes are slanted with respect to the applied field direction along  $z$  (There is a small in-plane field along the x-direction). We know from the experimental result that as the applied field is increased, the Q-vector of the magnetic Bragg peak moves to a lower value, but maintains its orientation of  $45^\circ$  with respect to beam direction. This indicates that the minority domain shrinks but the overall the stripe domain maintains the slant. Steps changes in multiple of 7 nm along  $L_x$  then means that periodicity changes perpendicular to the beam direction but along the small-in plane field direction take place in multiple of 7 nm. Interestingly, this value matches with the exchange length ( $L_{ex}$ ) of Fe/Gd thin film. One of the ways to think about this behavior is that as the minority domains shrink, there is a minimum distance between domain walls after which there cannot be smooth deformation of the spin texture. In the theory section we will show that indeed by defining a term that signifies ratio of spin kink to the spin chain, it is possible to predict jumps. At higher temperatures we observed an increase in the number of steps in the average-periodicity curves (see Fig.2(f and g) as a function of applied OOP field. This

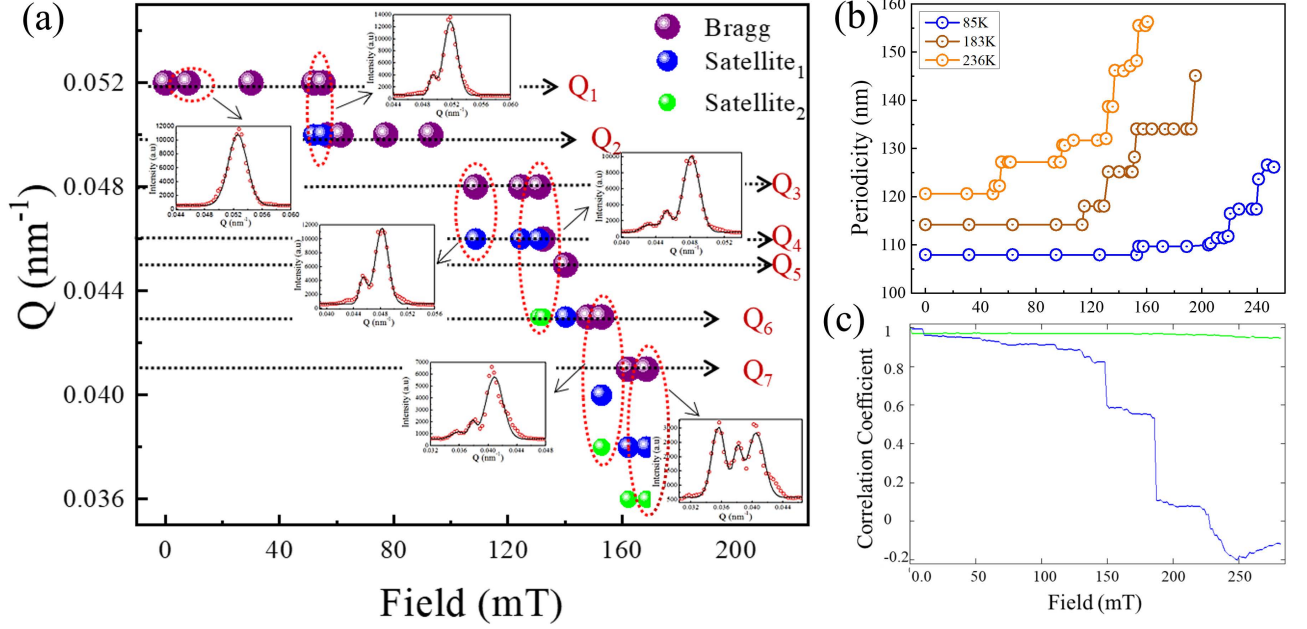


FIG. 2. **Evolution of stripe diffraction peak, periodicity and correlation with field.** (a) Plot of the q-vector of the satellite peaks as a function of the applied out-of-plane (OOP) magnetic field at 230 K as the system transitions from magnetic stripe phase to skyrmion phase. (b) Evolution of the stripe-periodicity with field at various temperatures showing discrete steps like feature. (c) Correlation coefficient values with respect to the remanent state (0 mT) for increasing magnetic field at 85K.

is due to fact that thermal fluctuations aids in faster transition from one step to the other as a result we obtain more number of steps at 236 K than 85 K even though the field range over which such steps occur is much higher at lower temperatures.

Existence of steps in solitonic systems with DMI has been observed experimentally and explained theoretically [19, 30]. The presence of DMI introduces a topologically protected kink in the spin texture. The topological protection of the kink means that there is an energy cost to kink-annihilation. Different topological sectors have different energy which is the reason for step-like features. In contrast, in Fe/Gd thin films the dominant interactions are exchange, dipole, and anisotropy. This supports an achiral magnetic structure. So far there has being no theoretical studies of the step-like behaviour on dipole interaction dominant achiral spin-structures in an amorphous system. In the theoretical model presented in the next section, we have mimicked the experimental conditions by investigating a one-dimensional dipolar mediated spin chain which is achiral in nature. We have numerically solved the Landau Lifshitz (LL) equation of motion to understand the magnetization dynamics observed in the Fe/Gd thin film experiment. Based on our calculations we show that the origin of the step like behaviour under the application of an external OOP magnetic field could be explained by the spin dynamic behavior of an achiral spin chain.

### Model and theory.

The spin kinks caused by long range dipolar interaction in the Fe/Gd thin film can be classified by a number  $n$ . In Fig. 4 we show the arrangement of spins in a finite-size chain under zero applied magnetic field with fixed boundary condition on

both ends. Both the local achiral structure and global achiral structure (describing the Fe/Gd thin film) are shown for comparison and context.

We consider a  $N$ -site 1D chain where spins interact with exchange interaction, dipolar interaction, PMA, and the in- and out- of plane magnetic field. The spin on each site is parameterized as

$$\mathbf{S}_i = (\sin \theta_i \cos \varphi_i, \sin \theta_i \sin \varphi_i, \cos \theta_i), \quad (2)$$

where the site spin angle  $\varphi_i = 2\pi ni/N$  and  $\theta_i = \frac{\pi}{2}$ . Here  $i = 0, 1, 2, \dots, N$  where  $N = N + 1$ . The kink sectors are classified by  $n$  which indicate the number of domains existing in the chain. The Hamiltonian for our Fe/Gd thin film is

$$H = H_J + H_D + H_K + H_h, \quad (3)$$

where the meaning and expression of each term is given by

$$H_J = -J \sum_{i \in N} \mathbf{S}_i \cdot \mathbf{S}_{i+1} \text{ (exchange)}, \quad (4a)$$

$$H_D = D \sum_{i,j \in \text{sc}} \mathbf{S}_i \cdot \mathbf{S}_j \Pi_{ij} \text{ (dipolar interaction)}, \quad (4b)$$

$$H_K = -K_U \sum_i (\mathbf{S}_i \cdot \mathbf{x})^2 \text{ (anisotropy)}, \quad (4c)$$

$$H_h = -g\mu_B H_x \sum_i S_i^x - g\mu_B H_y \sum_i S_i^y \text{ (magnetic field)}. \quad (4d)$$

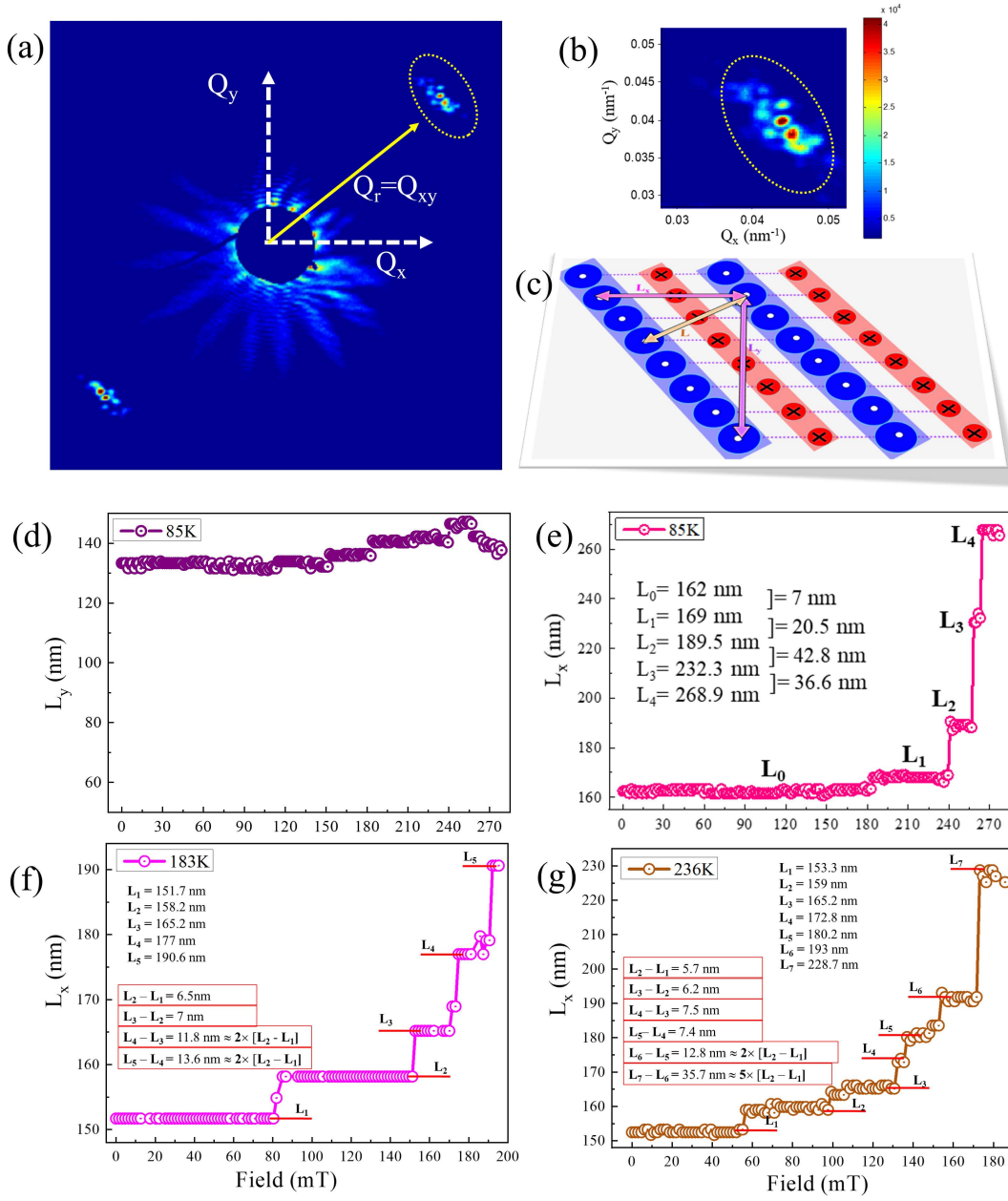


FIG. 3. **Stripe orientation and staircase-like behaviour.** (a) A typical scattering pattern of the stripe lattice along with the projection of the in-plane Q-vectors. (b) Enlarged image of the stripe-diffraction spot in Q-space. (c) Schematic real space view of the stripe-lattice orientation according to scattering image of Fig. 2(a), where blue circles with dot resemble the spin along the field direction while the red small circles with cross resemble the spins opposite to the field direction and  $L = L_x^2 + L_y^2$  corresponds to the periodicity of the stripe-lattice. Plot of the evolution of (d)  $L_y$  ( $= 2\pi/Q_y$ ) at 85 K and (e-g)  $L_x$  ( $= 2\pi/Q_x$ ) as a function of the applied magnetic field at  $T = 85$  K, 183 K and 236 K.

In the above  $i$  either denotes the lattice site in the 1D chain or the location of a spin site inside a supercell (sc). The exchange interaction strength is given by  $J$ , the dipolar interaction coupling by  $D$ , the anisotropy by  $K_U$ , and the in- and out-of plane magnetic field by  $H_x$  and  $H_y$ , respectively. The symbol  $g$  denotes the gyromagnetic ratio and the  $\mu_B$  is the Bohr magneton. The  $\Pi_{ij}$  in the dipolar interaction term is the Ewald coefficient which captures the long-range nature of the dipolar interaction. Using the angular representation of the spin  $S_i$  we can write the total energy as

$$\begin{aligned} \frac{H}{JS^2} = & - \sum_{i \in N} \cos(\varphi_{i+1} - \varphi_i) + J_d \sum_{i,j \in \text{sc}} \Pi_{ij} \cos(\varphi_i - \varphi_j) \\ & - K \sum_i \cos^2 \varphi_i - h_x \sum_i \cos \varphi_i - h_y \sum_i \sin \varphi_i, \end{aligned} \quad (5)$$

where we have now introduced the scaled variables  $J_d = \frac{D}{J}$ ,  $K = \frac{K_U}{J}$ ,  $h_x = \frac{g\mu_B H_x}{J}$  and  $h_y = \frac{g\mu_B H_y}{J}$ . In all our figures we will report the scaled fields in milli-units, that is,  $h_x = 1$  stands for

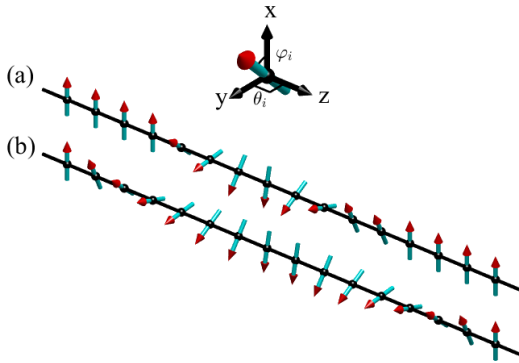


FIG. 4. **Local and global achiral spin structure.** Finite-size chains with local and global achiral magnetic order generated by the competition between exchange interaction and dipolar interaction are shown. (a) refers to local achiral magnetic order part of the chain exhibits achiral texture while (b) refers to a global achiral magnetic order where the entire chain length exhibits achiral rotation. This conceptual difference forms the basis for introducing our local coefficient  $T$ . The cartesian coordinate system shows the definition of the angle  $\varphi_i$  and the angle  $\theta$ . These represent the angles in the  $x$ - $y$  and the  $y$ - $z$  plane, respectively.

$10^{-3}$  scaled field units.

We implement the local achiral spin structure shown in Fig. 4(a) to perform the LL simulation. To mimic the finite size of the experimental sample and to allow for the domains to grow and collapse as observed experimentally, we utilized an embedding trick to simulate the LL equations-of-motion (EOM). To capture experimentally realistic sample conditions, from a computational perspective, we introduced the concept of a local coefficient  $T$ . From a physical perspective,  $T$  represents the ratio of the length of the achiral structure (which contains the twist sectors solely) over the length of the 1D chain. Thus, the achiral structure is embedded within a global ferromagnetic background spin texture. As we discuss later, the jumps occur due to the rearrangement of domain walls. The computational embedding trick allows us to capture the spontaneous rearrangement of the twist sectors in the chain configuration, thereby simulating the growth and collapse of the achiral domain walls. Our numerical simulations indicate that the eventual fate of the twist sectors and subsequent realization of jumps (as observed experimentally) is a subtle balance between  $J_d$ ,  $K$ , and  $N$ . We compute the minimum energy  $E_{min}$  using Eq. (5). The magnetization  $M$  is calculated using

$$M = \frac{1}{N} \sum_{i=0}^N \cos \varphi_i. \quad (6)$$

We present the energy and corresponding magnetization response of the local achiral state in Fig. 5. When the anisotropy is absent, we observe that the energy is degenerate for different twist sectors and no jumps are created by enhancing the dipolar interaction (see Fig. 5(a)-(c)). Moreover, it indicates that larger dipolar parameters induce a downshift in energy with

no visible effects on the magnetization behavior in the local achiral state. In the presence of anisotropy, we keep the dipolar interaction constant and increase the  $K$  parameter as shown in Fig. 5(c)-(e). We compute the LL dynamics on a chain of local achiral state with different anisotropy parameters. We find that upon enhancing anisotropy in the presence of a magnetic field, the energy degeneracy of the different twist sectors is broken with a simple upshift. With a relatively small  $T = \frac{1}{4}$  and a strong enough anisotropy  $K = 0.2$ , we observed jumps in both energy and magnetization in response to magnetic field as shown in Fig. 5(e).

In Fig. 5(f)-(j) we show our calculations of energy and magnetization response as  $T$  is varied. With decreasing  $T$ , jumps begin to happen in energy response with higher twist sector. When  $T > \frac{1}{2}$ , jumps happen in energy curves with  $n = 6$  as shown in Fig. 5(f)-(h). However, jumps happen in energy curves with smaller twist sectors  $n$  and lower magnetic field intensity  $h_x$ . In both Fig. 5(i) and Fig. 5(j), jumps happen when twist sector is  $n \geq 4$ . And the critical magnetic field intensity for the first jumps to happened decreases as  $T$  decreases. It is found that energy response is more powerful to show the disappearing of kinks while the jumps in magnetization response might caused by the position shifting of the kinks.

We considered a chain with larger number of sites. When the number of sites is  $N = 432$  and the dipolar parameter  $J_d = 0.00916$ , jumps can be observed in energy curve with twist sector  $n = 4$  and local coefficient  $T = \frac{1}{4}$ . However, no jumps can be observed with  $T = \frac{1}{3}$  and  $\frac{1}{2}$  (plots not shown). This behavior can also be seen in a system with  $N = 864$ . The result that the decreasing  $T$  contribute to the jumps, is also consistent with the  $N = 216$  system. Moreover, when the  $J_d$  increases, more kinks are able to establish and more jumps are observed. Thus, we draw a conclusion that not just the declining local coefficient  $T$ , but also the the rising dipolar parameter  $J_d$  results in the jumps happening in energy curve with smaller twist sector  $n$  and weaker magnetic field  $h_x$ .

There are no jumps in energy and magnetization response which are caused by kinks disappearing in the global achiral state (see Fig. 4(b) for global achiral state). The false jumps and oscillations in energy and magnetization for global achiral state are contributions from the position shifting of kinks. Hence, the 1D model in local achiral state is more capable to explain the origin of the jumps that happen in REXS experiment compared to the one in global achiral state.

### Discussion.

In this work we have shown experimentally that in a amorphous and achiral Fe/Gd magnetic thin film that exhibits aligned stripes, the domain periodicity changes in steps because of abrupt disappearance of domains. This result is interesting in itself because similar to DMI based solitonic system, exchange-dipole mediated Fe/Gd thin film system also shows similar step-like behavior even though global chirality is absent in the system. Since the presence of DMI can be ruled out in the Fe/Gd thin film [27, 28], there is no inherent topological protection for the stabilized magnetic structure [23]. Thus, the achiral nature of the system prevents it from generating topologically stable spin twist sectors. In this sense, the spin twists

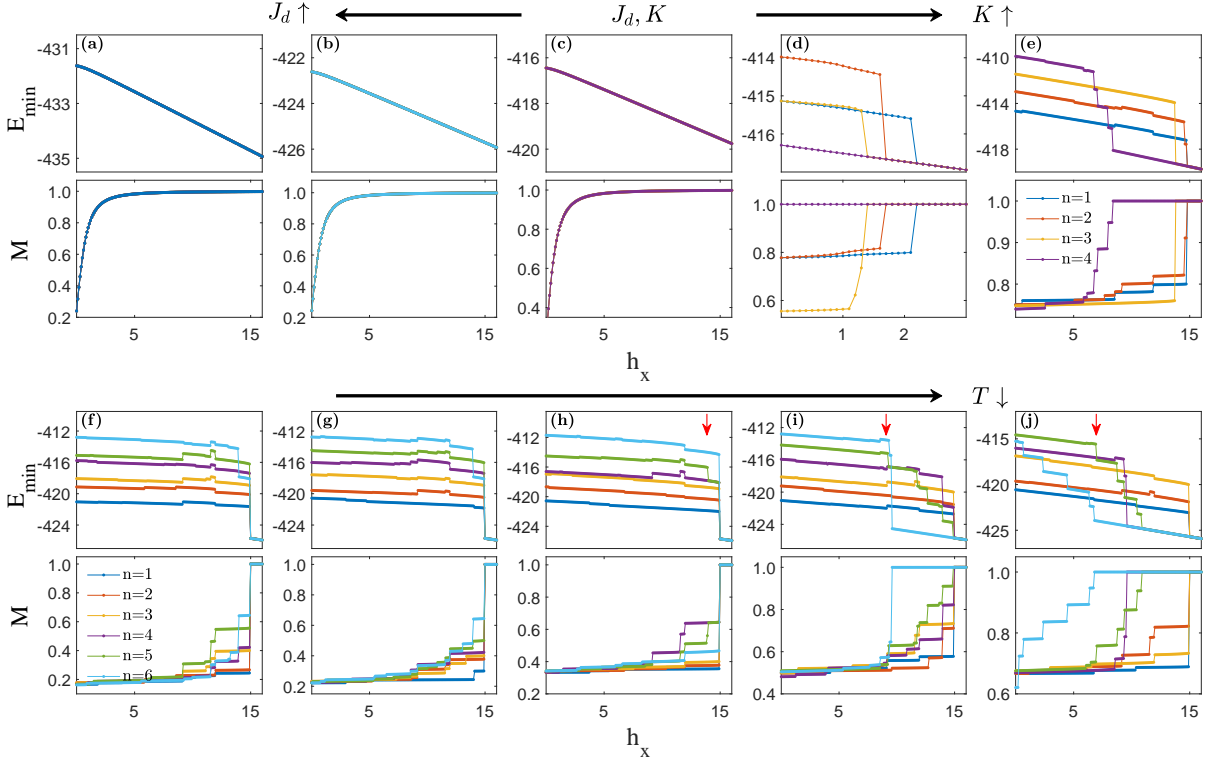


FIG. 5. **The energy and magnetization response for different  $T$  values.** In the upper panel, dipolar parameter is  $J_d = 0.00934$  and the anisotropy parameter is  $K = 0.2$  (c).  $J_d = 0.00962, 0.01004$  in (b) and (a) while anisotropy parameter  $K$  remains the same as the one in (c). Anisotropy parameter  $K = 0.1, 0.2$  in (d) and (e) while dipolar parameter remain the same as the one in (e). In the lower panel,  $J_d = 0.00962$  and  $K = 0.2$ . The local coefficients from the left to the right are  $T = \frac{7}{8}, \frac{7}{9}, \frac{2}{3}, \frac{1}{2}, \frac{1}{3}$ , respectively. Red arrows in (h)-(j) represent the first jump for energy curve with  $n = 5$ . The corresponding magnetic fields are  $h_x = 10.3, 9.2, 6.9$ . All results are calculated with the number of sites  $N = 216$ .

that are formed due to the competition between exchange and dipolar interaction should be smoothly transformed to the ferromagnetic ground state by any finite deformation.

The existence of steps, as observed in REXS experiments, indicates that along with global achirality there must be local structures with spin-twist characteristics. Intuitively, due to the achiral spin texture of the domains, as magnetic field is increased, the minority domain starts to shrink, resulting in two "like-domain" to come closer. The minimum distance between the two domains is guided by two spin-kinks on either side which should be equivalent to length of two domain walls. Using the well known formula  $l_w = \sqrt{J/K}$ , where  $l_w$  is the domain wall width, the domain wall width for Fe/Gd comes out  $\approx 3.2$  nm, twice of which is 6.4 nm, which is in close agreement to the experimental value of 7 nm. Thus the minimum distance between the two like-domains comes out to be equivalent to the exchange length ( $L_{ex}$ ) of the system from our experimental study. The above explanation also points to the existence of a "global" and "local" length scales in the system which will give rise to two energy scales. It is these competing energy scales that give rise to steps. Our system is reminiscent of the case of modulated periodicities.

We take the achiral nature of the stripe spin structure as an important point in our theoretical development and show that

the magnetization steps can indeed be observed in an achiral magnet. The variations and interplay of the length scales is captured in the parameter  $T$ . Analysis of the energy expression with different values of  $T$  suggests that in an achiral spin arrangement staircase structure can be observed only under certain specific ratios of 1D spin to spin-twist length scale. Although simplistic, our LL calculations using local achiral spin structure shown in Fig. 4(a) is able to capture the essential feature that the system has jumps in response to an external magnetic field. The jumps happen only when the anisotropy is presented. Absence of anisotropy leads to a degeneracy of energy response for different twist sectors, meaning absence of jumps in the system. Our study provides evidence and further impetus to study an achiral magnetic texture, both from an experimental and theoretical viewpoint.

**Acknowledgements.** J. L. and D. X. Yao are supported by NKRDP-2022YFA1402802, NKRDP-2018YFA0306001, NSFC-92165204, NSFC-11974432, and Shenzhen International Quantum Academy. This work in the USA was primarily supported by the U.S. Department of Energy, Office of Science, Office of Basic Energy Sciences, Materials Sciences and Engineering Division, under Contract no. DE-AC02-05-CH11231 within the Nonequilibrium Magnetic Materials Program (MSMAG). Work at the ALS, LBNL was supported by

the Director, Office of Science, Office of Basic Energy Sciences, of the US Department of Energy (Contract no. DE AC02-05CH11231). The research at UCSD was supported by the National Science Foundation, Division of Materials Research (Award #: 2105400). T. D. acknowledges hospitality of KITP. A part of this research was completed at KITP and was supported in part by the National Science Foundation under Grant No. NSF PHY-1748958. T.D. acknowledges helpful and insightful discussions on domain dynamics with Ulrich Rößler.

**Author contributions.** S.R. and A.S. conceived the experiment. A.S. and S.R. performed X-ray experiments. A.S., S.M. S.R. S.D.K. and P.F., analyzed the data and discussed experimental interpretation. S.A.M. and E.E.F. synthesized samples and performed magnetic characterization. The theory was conceived by T.D., J. L., and D. X.Y. J. L. performed the calculations. T.D and D.X.Y. checked the calculations. All authors contributed to the discussion and writing of the manuscript.

### Methods.

**Experimental details.** The coherent X-ray magnetic scattering measurements were performed at beamline 12.0.2.2 of the Advanced Light Source, LBNL. The incident beam was tuned to the Fe  $L_3$  edge (707 eV). Transverse coherence of the X-ray beam was established by inserting a 10  $\mu\text{m}$  pinhole in the beam path before the sample. The scattering experiment was done in the transmission geometry at temperatures ranging from 40 K to 300 K as a function of the OOP magnetic field from 0 mT to 500 mT. (Fig. 1(a)). The sample was subjected to the following initial magnetic field protocol. First the field was raised to 500 mT, then lowered to -500 mT and finally to zero before taking the measurements. The field ramp rate for the first two legs is 13 mT/sec, while the final drop of field from -500 mT to 0 mT took place at a rate of 380 mT/sec. We start our measurement at this zero-field condition and proceed to measure the diffraction signal as a function of applied magnetic field at a constant rate of 1.575 mT/s. A Charge Coupled Device (CCD) camera placed at about 0.5 m downstream of the sample was used to record the scattered intensity patterns.

### Theoretical method.

*Ewald method.* In the Hamiltonian calculation, Ewald summation is applied, which is given by

$$\begin{aligned} \Pi_{ij} = & \sqrt{\frac{2}{\pi}} \frac{1}{3\sigma^3} \sum_n e^{-\frac{|r_{ij}-nL|^2}{2\sigma^2}} + \frac{4\pi}{\Omega} \sum_{k \neq 0} e^{-\frac{\sigma^2 k^2}{2}} \cos(kr_{ij}) \\ & - \sqrt{\frac{2}{\pi}} \frac{1}{3\sigma^3} \delta_{ij}, \end{aligned} \quad (7)$$

where  $r_{ij}$  represents the distance between two spin sites,  $L$  is the size of the supercell,  $n$  is the supercell label,  $\sigma$  is the real-space cut-off,  $k$  is the momentum space label, and  $\Omega$  is the volume of the supercell which in our case is equal to  $L$ . The Ewald parameter will be redefined as  $\Pi_{ij} = \Pi_{|i-j|} \equiv \Pi_m$ , where the symbol  $m$  tracks the number of Ewald parameters for the specific supercell size choice. The values of  $\Pi_m$  are shown in Table. I.

*Landau-Lifshitz (LL) equation of motion.* We perform a LL EOM spin dynamics calculation on Eq. 3. We obtained an it-

TABLE I. Ewald parameter symbols and the corresponding Ewald parameter values given by Eq. 7.

Ewald parameter symbol	Ewald parameter value
$\Pi_1$	2.00
$\Pi_2$	1.72
$\Pi_3$	1.32
$\Pi_4$	0.85
$\Pi_5$	0.38

TABLE II. Maximum allowed number of kink sectors  $n_{max}$  under different scaled dipolar parameter  $J_d$  for a given number of lattice sites  $N$ . We introduce a sector  $n$  denoting the number of twisted magnetic structures in a achiral lattice. The system relaxes to the ground state with a maximal sector value  $n_{max} = \left\lfloor \frac{N\Delta\varphi}{2\pi} \right\rfloor$ , where the square bracket implies the flooring function.

Number of sites	Dipolar $J_d$	Sector $n_{max}$
216	0.00934	4
	0.00962	6
	0.01004	8
432	0.00916	4
	0.00934	8
	0.00962	12
864	0.00916	8
	0.00934	17
	0.00962	25

erative equation which can be used to calculate the angle  $\varphi_i$  of each spin on the chain. Based on our computations, we are able to generate a stabilized spin order along the chain. Next, we computed the twist angle  $\Delta\varphi$  of the ground state in the absence of an external magnetic field using the energy minimization condition for the supercell given by the expression

$$\frac{E}{JS^2} = -\cos \Delta\varphi + J_d \sum_{m=1}^{L-1} (L-m) \cos(m\Delta\varphi) \Pi_m. \quad (8)$$

The angle  $\varphi_i$  was analyzed to obtain the relationship between the range of  $J_d$  and the number of kinks for a given lattice size of site  $N$ . The relationship between the number of sites  $N$ , dipolar parameter  $J_d$  and the maximal sector  $n_{max}$  is shown in Table. II. Note that to perform the calculation, one needs to choose a supercell size that stabilizes the ground state and ensures that there will be minimal to no numerical oscillations in the computed result due to convergence issues. We found that  $L = 6$  is the optimal supercell size which yields numerically stable results for our LL analysis. Using the numerically stable data, we computed the minimum energy  $E_{min}$  (scaled relative to  $JS^2$ ) and magnetization  $M$  (scaled relative to  $S$ ). To compare our numerical results with the experimental setup of the multilayer Fe-Gd system, we need to mimic the experimental conditions. Therefore, all the results are calculated by applying a tiny in-plane field  $h_y$ .

The two angular variable EOMs are given by (for  $\hbar = 1$ )

$$S \sin \theta_i \partial_t \theta_i = \frac{\partial H}{\partial \varphi_i}, \quad S \sin \theta_i \partial_t \varphi_i = -\frac{\partial H}{\partial \theta_i}, \quad (9)$$

where only the first equation is required because the angle  $\theta$  is held constant. Using Eq. (9) we can obtain the following expressions

$$0 = \frac{1}{2} [\sin(\varphi_i - \varphi_{i-1}) - \sin(\varphi_{i+1} - \varphi_i)] \\ + J_d \sum_{j \in sc} [\sin(\varphi_{i+|i-j|} - \varphi_i) - \sin(\varphi_i - \varphi_{i-|i-j|})] \Pi_{ij} \quad (10) \\ + 2K \sin \varphi_i \cos \varphi_i + h_x \sin \varphi_i - h_y \cos \varphi_i.$$

The above can be split further into a form convenient for a numerical iterative self-consistent approach to solve for the angle  $\phi_i$ . Hence, we write

$$A_i = \frac{1}{2} (\sin \varphi_{i+1} + \sin \varphi_{i-1}) - J_d \sum_{j \in sc} (\sin \varphi_{i+|i-j|} \\ + \sin \varphi_{i-|i-j|}) \Pi_{ij} - K \sin \varphi_i + h_y \quad (11a)$$

$$B_i = \frac{1}{2} (\cos \varphi_{i+1} + \cos \varphi_{i-1}) - J_d \sum_{j \in sc} (\cos \varphi_{i+|i-j|} \\ + \cos \varphi_{i-|i-j|}) \Pi_{ij} + K \cos \varphi_i + h_x, \quad (11b)$$

with the site angle  $\varphi_i$  is defined as

$$\sin \varphi_i = \frac{A_i}{\sqrt{A_i^2 + B_i^2}}, \quad \cos \varphi_i = \frac{B_i}{\sqrt{A_i^2 + B_i^2}}. \quad (12)$$

The LLG equation is solved with the boundary condition  $\varphi_0 = 0$  and  $\varphi_N = 2\pi n$ .

- 
- [1] K. von Klitzing, T. Chakraborty, P. Kim, V. Madhavan, X. Dai, J. McIver, Y. Tokura, L. Savary, D. Smirnova, A. M. Rey, C. Felser, J. Gooth, and X. Qi, *Nature Reviews Physics* **2**, 397 (2020).
- [2] G. Gruner, *Density Waves In Solids (1st ed.)* (CRC Press, 2000).
- [3] S. Lee, E. W. Huang, T. A. Johnson, X. Guo, A. A. Husain, M. Mitrano, K. Lu, A. V. Zakrzewski, G. A. de la Peña, Y. Peng, H. Huang, S.-J. Lee, H. Jang, J.-S. Lee, Y. I. Joe, W. B. Doriese, P. Szypryt, D. S. Swetz, S. Chi, A. A. Aczel, G. J. MacDougall, S. A. Kivelson, E. Fradkin, and P. Abbamonte, *Proceedings of the National Academy of Sciences* **119**, e2119429119 (2022), <https://www.pnas.org/doi/pdf/10.1073/pnas.2119429119>.
- [4] J. M. Tranquada, B. J. Sternlieb, J. D. Axe, Y. Nakamura, and S. Uchida, *Nature* **375**, 561 (1995).
- [5] S. A. Kivelson, I. P. Bindloss, E. Fradkin, V. Oganesyan, J. M. Tranquada, A. Kapitulnik, and C. Howald, *Rev. Mod. Phys.* **75**, 1201 (2003).
- [6] C. H. Chen and S.-W. Cheong, *Phys. Rev. Lett.* **76**, 4042 (1996).
- [7] B. Binz and A. Vishwanath, *Phys. Rev. B* **74**, 214408 (2006).
- [8] P. Bak and R. Bruinsma, *Phys. Rev. Lett.* **49**, 249 (1982).
- [9] Aubry, S., *J. Phys. France* **44**, 147 (1983).
- [10] C. Reichhardt and F. Nori, *Phys. Rev. Lett.* **82**, 414 (1999).
- [11] P. Bak, *Journal of Applied Physics* **50**, 1970 (1979), <https://doi.org/10.1063/1.327129>.
- [12] T. Matsuda, S. Partzsch, T. Tsuyama, E. Schierle, E. Weschke, J. Geck, T. Saito, S. Ishiwata, Y. Tokura, and H. Wadati, *Phys. Rev. Lett.* **114**, 236403 (2015).
- [13] A. A. Fraerman and M. V. Sapozhnikov, *Phys. Rev. B* **65**, 184433 (2002).
- [14] K. Kuroda, Y. Arai, N. Rezaei, S. Kunisada, S. Sakuragi, M. Alaei, Y. Kinoshita, C. Bareille, R. Noguchi, M. Nakayama, S. Akebi, M. Sakano, K. Kawaguchi, M. Arita, S. Ideta, K. Tanaka, H. Kitazawa, K. Okazaki, M. Tokunaga, Y. Haga, S. Shin, H. S. Suzuki, R. Arita, and T. Kondo, *Nature Communications* **11**, 2888 (2020).
- [15] C. Bahr, D. Fliegner, C. J. Booth, and J. W. Goodby, *Phys. Rev. E* **51**, R3823 (1995).
- [16] Z. Li, Z. Fu, H. Cai, T. Hu, Z. Yu, Y. Luo, L. Zhang, H. Yao, X. Chen, S. Zhang, G. Wang, X. Dong, and F. Xu, *Science Advances* **8**, eabl9088 (2022), <https://www.science.org/doi/pdf/10.1126/sciadv.abl9088>.
- [17] N. S. Kiselev, A. N. Bogdanov, R. Schäfer, and U. K. Röbller, *Journal of Physics D: Applied Physics* **44**, 392001 (2011).
- [18] J.-i. Kishine, I. G. Bostrem, A. S. Ovchinnikov, and V. E. Sinityn, *Phys. Rev. B* **86**, 214426 (2012).
- [19] J.-i. Kishine, I. G. Bostrem, A. S. Ovchinnikov, and V. E. Sinityn, *Phys. Rev. B* **89**, 014419 (2014).
- [20] S. Mühlbauer, B. Binz, F. Jonietz, C. Pfleiderer, A. Rosch, A. Neubauer, R. Georgii, and P. Böni, *Science* **323**, 915 (2009), <https://www.science.org/doi/pdf/10.1126/science.1166767>.
- [21] Y. Tokura and N. Kanazawa, *Chemical Reviews*, *Chemical Reviews* **121**, 2857 (2021).
- [22] Y. Togawa, Y. Kousaka, K. Inoue, and J.-i. Kishine, *Journal of the Physical Society of Japan* **85**, 112001 (2016).
- [23] Togawa, Yoshihiko, Inoue, Katsuya, Kishine, Jun-ichiro, Kousaka, and Yusuke, *Journal of the Physical Society of Japan* (2016).
- [24] Y. Togawa, Y. Kousaka, S. Nishihara, K. Inoue, J. Akimitsu, A. S. Ovchinnikov, and J. Kishine, *Phys. Rev. Lett.* **111**, 197204 (2013).
- [25] Y. Togawa, T. Koyama, Y. Nishimori, Y. Matsumoto, S. McVitie, D. McGruther, R. L. Stamps, Y. Kousaka, J. Akimitsu, S. Nishihara, K. Inoue, I. G. Bostrem, V. E. Sinityn, A. S. Ovchinnikov, and J. Kishine, *Phys. Rev. B* **92**, 220412 (2015).
- [26] M. N. Wilson, E. A. Karhu, D. P. Lake, A. S. Quigley, S. Meynell, A. N. Bogdanov, H. Fritzsche, U. K. Röbller, and T. L. Monchesky, *Phys. Rev. B* **88**, 214420 (2013).
- [27] S. A. Montoya, S. Couture, J. J. Chess, J. C. T. Lee, N. Kent, D. Henze, S. K. Sinha, M.-Y. Im, S. D. Kevan, P. Fischer, B. J. McMorran, V. Lomakin, S. Roy, and E. E. Fullerton, *Phys. Rev. B* **95**, 024415 (2017).
- [28] J. C. T. Lee, J. J. Chess, S. A. Montoya, X. Shi, N. Tamura, S. K. Mishra, P. Fischer, B. J. McMorran, S. K. Sinha, E. E. Fullerton, S. D. Kevan, and S. Roy, *Applied Physics Letters* **109**, 022402 (2016), <https://doi.org/10.1063/1.4955462>.
- [29] A. Singh, J. C. T. Lee, K. E. Avila, Y. Chen, S. A. Montoya, E. E. Fullerton, P. Fischer, K. A. Dahmen, S. D. Kevan, M. K. Sanyal, and S. Roy, *Nature Communications* **10**, 1988 (2019).
- [30] Y. Togawa, T. Koyama, Y. Nishimori, Y. Matsumoto, S. McVitie, D. McGruther, R. L. Stamps, Y. Kousaka, J. Akimitsu, S. Nishihara, K. Inoue, I. G. Bostrem, V. E. Sinityn, A. S. Ovchinnikov, and J. Kishine, *Phys. Rev. B* **92**, 220412 (2015).